agronomy

MDPI

Article

Study on Water and Salt Transport Characteristics of Sunflowers under Different Irrigation Amounts in the Yellow River Irrigation Area

Changfu Tong [1,2], Rui He [1,2,*], Jun Wang [1] and Hexiang Zheng [1]

[1] Institute of Pastoral Water Resources Science, Ministry of Water Resources, Hohhot 010020, China; tongcf@iwhr.com (C.T.); slwj1988@iwhr.com (J.W.); mkszhx@iwhr.com (H.Z.)
[2] College of Water Resources and Civil Construction Engineering, Inner Mongolia Agricultural University, Hohhot 010018, China
* Correspondence: hehe66524@emails.imau.edu.cn

Abstract: The control of irrigation volume is of significant importance in arid regions of northwest China. Particularly, it has a crucial impact on the salinization of shallow groundwater areas. In 2022 and 2023, field experiments were conducted to test three distinct under-membrane irrigation treatments. These treatments were assigned water quotas of HW (27 mm), MW (22.5 mm), and LW (18 mm). The HYDRUS-2D model was integrated with a field experiment to accurately simulate the dynamic fluctuations of soil water and salt in the sunflower root zone. The model's performance was assessed and verified using real-field data from 2022 and 2023, and the simulation results closely matched the measured values. This research also used stable hydroxide isotopes to assess the water supply from various soil layers at different time intervals in sunflower plants. The results indicated that the three different levels of irrigation applied under the membrane had a significant impact on soil water content. Specifically, there was a significant difference in soil water content at a depth of 0–40 cm ($p < 0.05$), while there was little effect on the water content at a depth of 40–60 cm ($p > 0.05$). After irrigation, the average salt content in the top 0–20 cm of soil decreased by 7.0% compared to the medium and low irrigation levels, and by 10.8% compared to the medium irrigation level. Additionally, the medium irrigation level resulted in a 10.8% decrease in salt content compared to the low irrigation level, and a 4.1% decrease compared to the medium irrigation level. During the same period, the soil salinity levels at depths of 0–20 cm, 20–40 cm, 40–60 cm, and 60–100 cm in the area outside the membrane were measured to be 2.7~4.8 g·kg^{-1}, 2.8~4.0 g·kg^{-1}, 2.7~3.4 g·kg^{-1}, and 1.7~2.6 g·kg^{-1}, respectively. These levels decreased by 13.1~55.5%, 0.7~42.8%, −0.4~16.2%, and −72.7~7.5%, respectively. Following irrigation, the HW treatment mostly absorbed water in the 0–40 cm soil layer, while the MW and LW treatments absorbed water in both the 0–40 cm and 60–80 cm soil levels. The results indicated that the most optimal drip irrigation method beneath the membrane in this location was achieved when the amount of water applied was between 25–30 mm. This method demonstrated a combination of water conservation, high crop yield, and effective salt suppression.

Keywords: HYDRUS-2D model; hydrogen and oxygen isotopes; soil water salinity; water use efficiency; Yellow River Irrigation District

Citation: Tong, C.; He, R.; Wang, J.; Zheng, H. Study on Water and Salt Transport Characteristics of Sunflowers under Different Irrigation Amounts in the Yellow River Irrigation Area. *Agronomy* **2024**, *14*, 1058. https://doi.org/10.3390/agronomy14051058

Academic Editors: Robert J. Lascano and Maomao Hou

Received: 15 April 2024
Revised: 9 May 2024
Accepted: 14 May 2024
Published: 16 May 2024

1. Introduction

Water shortage and soil salinization are significant limitations to agricultural growth on a global scale [1,2]. This issue hampers the development of crops, diminishes agricultural productivity and quality, lowers the efficiency of fertilizer use, and has negative impacts on both the sustainable exploitation of soil and ecological integrity [3,4]. Various measures have been implemented sequentially in nations including Israel, the United States, and India

to tackle this issue. Saline–alkaline land management has received significant attention in the northwestern region of China in recent years.

The irrigation area located on the southern bank of the Yellow River in the Inner Mongolia Autonomous Region is a prime example of a region with limited water resources and high levels of soil salinization. The cultivated area spans around 178,000 hm^2, with over half of the land being affected by salinization. Furthermore, this issue is persistently growing. Surface irrigation, specifically border irrigation, has been used in this region in recent years to enhance soil quality. The primary objective is to flush out salts from the soil, therefore mitigating their negative impact on crops and ultimately boosting agricultural yields [5]. This technique can rapidly remove salt from the soil, but it may lead to an increase in the groundwater level, resulting in the re-salinization of the soil [6]. Simultaneously, the irrigation region is confronted with the issue of water scarcity, making it crucial to achieve the logical and effective use of water resources in farms. The sub-membrane drip irrigation technique is a widely used method for conserving water. It is particularly successful in irrigating salty soil. The primary function of the performance is as follows [7–12]: (1) mitigating soil salt stress by applying pressure salt; (2) enhancing the beneficial cycle of farming soil; (3) providing heat preservation and moisture to support crop development; and (4) enhancing water usage efficiency.

Integrating field experiments with numerical modeling may provide an easier and more efficient approach to acquiring, forecasting, and verifying the dynamic alterations of water and salt in agricultural areas. Currently, the predominant numerical models used to study the dynamic changes in soil water and salt in agricultural fields are HYDRUS (2D/3D), SWAP, AquaCrop, and SWAT. These models effectively simulate the processes of soil moisture and solute transport [13–16]. SWAP, AquaCrop, and SWAT are often used for modeling hydrological conditions and soil nitrogen levels in agricultural areas. HYDRUS (2D/3D) outperforms in mimicking soil moisture and salt levels in farms. The model incorporates adaptable boundary conditions and effectively replicates the dynamics of 2D unsaturated soil moisture and salt transport processes [17,18]. A study [19] employed HYDRUS-2D to model the moisture and pore conductivity of olive orchards in desert conditions. The results demonstrated a high level of accuracy, offering valuable insights into the irrigation management of olive orchards in such environments. However, the study did not analyze the soil water fluxes, indicating the need for further research on water resource management. Elnesr et al. [20] utilized the HYDRUS-2D model to simulate the water content and pore conductivity of maize under different irrigation regimes during the reproductive period. They aimed to minimize inefficient water usage and suggest an appropriate irrigation plan for maize growth. However, there is limited research on soil solutes and fluxes during the reproductive period of maize. The process of water and solute changes in the soil profile, as well as the distribution of crop root development and water absorption under drip irrigation, may be better understood by modeling water and solute transport. This plays a crucial role in studying these phenomena [21–25].

Several researchers [26–28] have investigated the movement of water and salt in soil by integrating field data with HYDRUS simulation. This approach aims to create effective methods for managing water and salt in agricultural fields. The HYDRUS (2D/3D) model is particularly advantageous in accurately simulating the dynamics of soil water and salt. Nevertheless, the HYDRUS model is unable to accurately identify the source of soil water for root water uptake. Additionally, it cannot determine water utilization in various soil layers. Its capabilities are restricted to assessing water fluctuations in different soil layers to identify the primary water uptake layer for crops. However, understanding the contribution of water sources in different soil layers is crucial for irrigation crops with shallow underground water burial areas and their root water uptake.

Stable hydroxide isotopes may serve as natural tracers to monitor the transport of water in soil. Information on water mobility in soil may be acquired by examining the variations in stable hydroxide isotopes in soil water [29]. In recent years, numerous scholars have made significant advancements in this field. For instance, Xing Xing et al. [30]

analyzed the contribution of various water sources to desert plants. They achieved this by determining the stable hydroxide isotope values of xylem water from five dominant plants and different potential water sources. Similarly, Pei Yanwu et al. [31] examined the hydroxide isotope values of xylem water from three plantations in Maowuosu Sandy Land at different underground water levels. Their study concluded that the contribution of shallow groundwater to the recharge of deep soil water can partially alleviate the soil water deficit during the dry season. Prior authors mostly used a single model or approach to examine the water and solute conditions in the root zone of crops. However, this approach has inherent limitations and fails to provide a thorough analysis of the combined dynamics of crops with regard to water and salt.

This study aims to utilize the HYDRUS-2D model to simulate and analyze the movement of soil water and salt in the root zone of sunflowers in an irrigation area with shallowly buried underground water. Additionally, stable hydrogen and oxygen isotopes will be incorporated to precisely determine the water uptake and utilization of sunflowers in different soil layers during various fertility stages. The simultaneous use of both strategies will provide pragmatic and theoretical assistance for the cultivation of sunflowers in regions characterized by a limited depth of subterranean water. Furthermore, this work employs the HYDRUS-2D model to conduct a scenario analysis to investigate the appropriate quantity of irrigation water that is suited for the area. The main contributions of this study are twofold. Firstly, it involves the evaluation and validation of the HYDRUS-2D model using various types of data, including soil water, salt, and stable hydroxide isotopes. Additionally, it conducts a detailed analysis of the changes in soil water and salt within the root zone of sunflowers, as well as the amount of water supplied by different soil layers during each fertility period of sunflowers under different irrigation quotas. Secondly, it aims to determine the proportional equilibrium of soil water and salt within the underground water–soil–plant system under different irrigation rates and crop yields.

2. Materials and Methods

2.1. Overview of the Experimental Area

The experimental region is situated in the Yellow River Water Drip Irrigation Water Conservation and Efficiency Experimental region of Dalate Banner, Ordos City, Inner Mongolia Autonomous Region. The co-ordinates of the location are 40°29′32″ N, 109°53′10″ E, with an elevation of 1009 m. The location of the experimental area is shown in Figure 1. The Inner Mongolia Yellow River South Bank Irrigation District is one of the six major yellow diversion irrigation districts in the Inner Mongolia Autonomous Region. It is an important commodity grain base owned by both the state and the autonomous region. The irrigation district is situated in the northern part of Ordos City and is distributed in a narrow east–west strip. It has a typical temperate continental climate with semi-arid characteristics, characterized by large temperature differences between day and night and periodic rainfall and heat. The long-term average temperature is 6.2 °C, while the average annual precipitation is 348.3 mm. The majority of the precipitation occurs between July and September, accounting for approximately 70% of the total annual precipitation. Over the years, the average evaporation rate is around 2506.3 mm, which is roughly seven times higher than the amount of precipitation. The soil consists mostly of loamy and clay loam textures. The organic matter, total salt, nitrate nitrogen, and ammonium nitrogen content in the soil, within the 0–100 cm depth, are measured at 12.1 $g \cdot kg^{-1}$, 1.0 $g \cdot kg^{-1}$, 6.2 $mg \cdot kg^{-1}$, and 3.5 $mg \cdot kg^{-1}$, respectively.

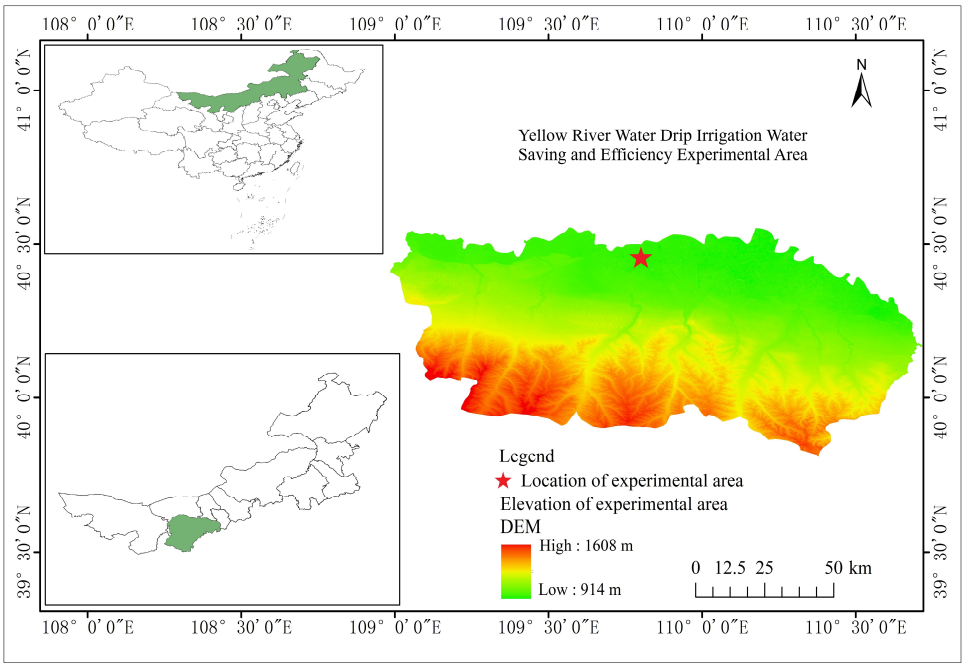

Figure 1. Geographic location of the experimental area.

2.2. Experimental Design

The experiment was conducted on a plot with drip irrigation covered by a film. Three different irrigation quota treatments were established for under-film drip irrigation, with three replications for each treatment, resulting in a total of nine treatments. The three irrigation quota treatments were as follows: 1.2 times the local level—HW (27 mm), the local level—MW (22.5 mm), and 0.8 times the local level—LW (18 mm), respectively. The irrigation schedule in the local irrigation region was determined based on the knowledge and expertise of farmers and ranchers. Irrigation was carefully scheduled and regulated, and the water used for irrigation was sourced from the Yellow River, with a total dissolved solids (TDS) concentration of 0.59 $g \cdot L^{-1}$.

The sunflower crop had six watering events throughout each reproductive phase in each year of the experiment. The irrigation method used is shown in Table 1. The dimensions of each experimental plot were 25 m in length and 6 m in width. To mitigate the potential interference from neighboring plots, a protective zone measuring 1 m in width and running north–south was established on both the east and west sides of each plot. Additionally, a 2.5 m-wide protective zone was designated at both ends of the experimental area. These protective zones were subjected to identical tillage, fertilizer application, and other treatments as the main plots. The sunflower crop was planted in early June of both 2022 and 2023. A spring irrigation treatment was applied 10 days before planting, and the crop was collected in early October of both years. The experimental variety used is "Jinyu 63". The planting method involves utilizing a film with two rows, with a spacing of 135 cm for laying the drip irrigation belt. The film width is 70 cm, and the broad row spacing is 90 cm, while the narrow rows have a spacing of 45 cm. The sowing volume is controlled at around 30,000 plants per ha. Please refer to Figure 2 for the experimental arrangement.

An experiment was conducted to test the effectiveness of drip irrigation using a pump. The experimental irrigation was conducted using a drip irrigation system. The water was sourced from a channel, filtered, and then pumped into the experimental plot through a low-pressure infiltration microfiltration system. The irrigation was carried out using a patch drip irrigation belt with a pipe diameter of 16 mm (Yurun Pipe Industry Co., Ltd., Heze, China). The flow rate of the water was 1.60 $L \cdot h^{-1}$, and the spacing between the drip heads was 30 cm. The irrigation water quantity for each treatment was regulated using a water meter and a valve.

Table 1. Irrigation time and water allocation.

Year of Experiment	Treatment	Irrigation Time	Irrigation Quota (mm)	Total Irrigation Quota (mm)
2022	HW	6.20, 7.15, 7.28, 8.11, 8.24, 9.08	27	162
	MW	6.20, 7.15, 7.28, 8.11, 8.24, 9.08	22.5	135
	LW	6.20, 7.15, 7.28, 8.11, 8.24, 9.08	18	108
2023	HW	6.18, 7.14, 7.29, 8.13, 8.25, 9.06	27	162
	MW	6.18, 7.14, 7.29, 8.13, 8.25, 9.06	22.5	135
	LW	6.18, 7.14, 7.29, 8.13, 8.25, 9.06	18	108

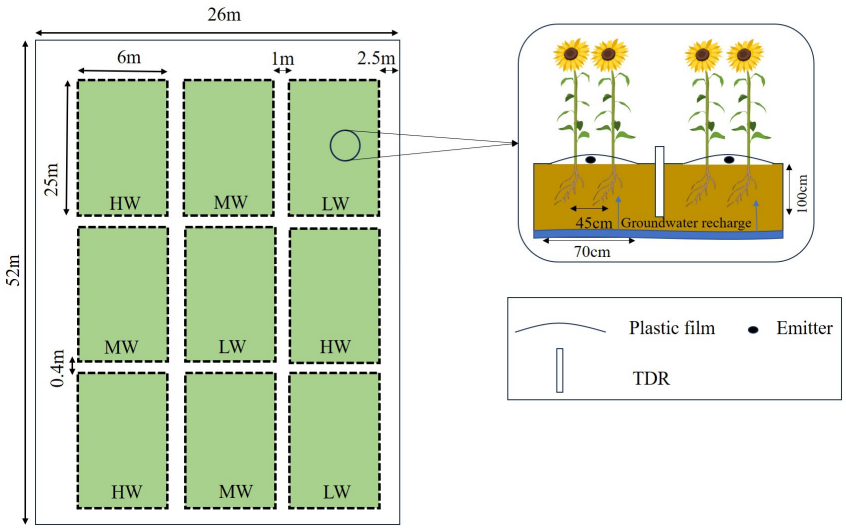

Figure 2. Schematic diagram of planting.

2.3. Data Observation and Computation

2.3.1. Meteorological Data

Hourly meteorological data, such as air temperature, rainfall, air humidity, solar radiation, atmospheric pressure, and wind speed, were gathered in the experimental region using automated weather stations (Tian Qiong Co., Ltd., Weifang, China). The Penman–Monteith formula [32] was used to calculate crop evapotranspiration (ET_0). The potential crop evapotranspiration (ET_P) is determined by multiplying ET_0 with the crop coefficient (Kc) for sunflowers. According to data from FAO56, the recommended values for Kc at the beginning, middle, and end of sunflower fertility are 0.35, 1.1, and 0.4, respectively. In the HYDRUS-2D model, ET_P is the sum of potential evaporation (E_P) and potential transpiration (T_P), which is calculated using the following equation [33]:

$$ET_P = E_P + T_P \quad (1)$$

$$E_P = ET_P \cdot e^{-k \cdot LAI} \quad (2)$$

$$T_P = \left(1 - e^{-k \cdot LAI}\right) ET_P \quad (3)$$

where k is the extinction coefficient and LAI is the leaf area index.

2.3.2. Groundwater Level

Observation wells (Oneset Co., Ltd., London, UK) in each plot were equipped with automatic water level recorders, which had an inner diameter of 20 cm and a depth of 4 m. To monitor the real-time groundwater level condition, data were captured every other day and saved in the recorders, as shown in Figure 3.

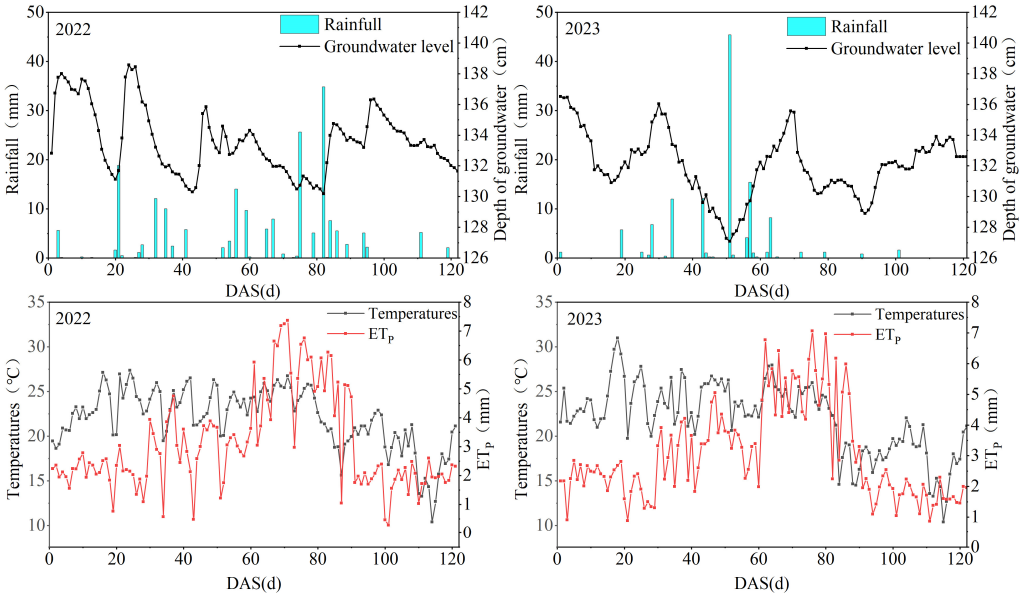

Figure 3. Depth to groundwater (cm), rainfall (mm) potential evapotranspiration (mm), and air temperature (°C) for the test years ((**left**) 2022, (**right**) 2023).

2.3.3. Soil Water Content and Electrical Conductivity (EC)

Soil samples were obtained from the soil layer that extends from 0 to 100 cm below the surface. A soil auger with a diameter of 3 cm and a length of 1.3 m was used to collect the samples. The soil samples were categorized into five layers based on depth: 0–20 cm, 20–40 cm, 40–60 cm, 60–80 cm, and 80–100 cm. These samples were then placed in a designated aluminum container and sent to the laboratory. In the laboratory, the water content of the soil samples was measured using an electronic scale with a precision of 0.01 g.

The electrical conductivity (EC) of the filtrate, obtained by mixing soil and water in a mass ratio of 1:5, was measured using a DDS-307A conductivity meter manufactured by Shanghai Yidian Scientific Instrument Co., Ltd. in Shanghai, China. The duration for measuring the soil water content and electrical conductivity was 4 to 6 days. The calculation of soil salinity was performed using the provided soil electrical conductivity (EC) measurements, according to the following formula:

$$Y = 5.1949EC_{1:5} + 0.0685 \quad (4)$$

where Y is the total soil salt in g·kg^{-1}; and $EC_{1:5}$ is the EC value of soil leachate mixed with water in ds·m^{-1} when the soil and water mass ratio is 1:5.

2.3.4. Soil Salinity Changes

Soil samples were gathered from each experimental plot and the level of soil salinity was assessed about every 10 days, with extra tests taken before and after irrigation. The impact of soil salt buildup and desalination may be seen by calculating the ratio between the difference in soil salinity measurements at the beginning and end, and the original soil salinity.

$$N = \frac{x_1 - x_2}{x_1} \times 100\% \quad (5)$$

where N is the rate of change of soil salinity, with negative values indicating salt accumulation and positive values indicating desalination, %; and x_1 and x_2 represent soil salinity before and after irrigation, g·kg^{-1}, respectively.

2.3.5. Leaf Area, Plant Height, and Yield of Sunflower

Within each experimental plot, excluding side rows, seven sunflowers in optimal growth conditions were chosen at random. Their height, leaf breadth, and leaf length were then measured using a tape measure with a precision of 0.1 cm. The leaf area index was determined by multiplying 0.75 with the product of the leaf width and leaf length. The yield-to-crop evapotranspiration water consumption (ET_C) ratio [34] was calculated in the middle of each experimental plot by randomly sampling 20 healthy plants after sunflower maturity. Sunflower plant height and leaf area index are shown in Figure 4.

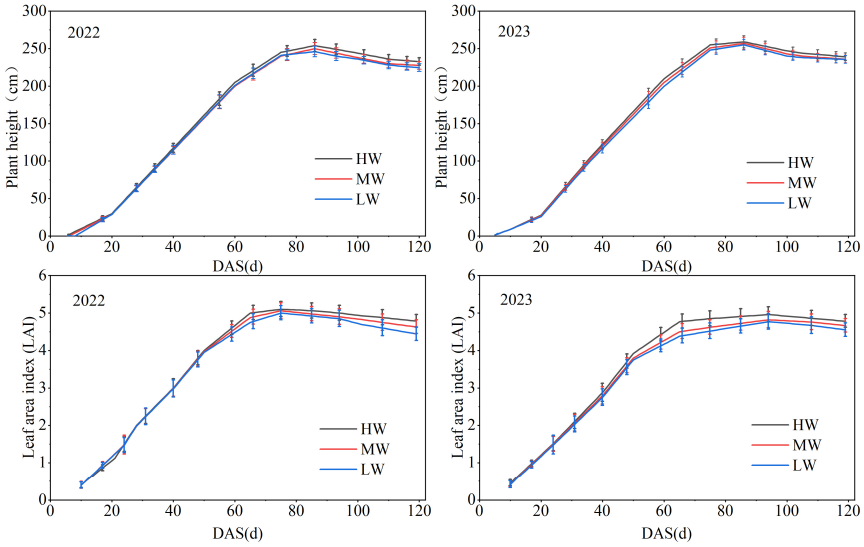

Figure 4. Changes in plant height and leaf area of sunflowers under different drip irrigation rates in the experimental years (2022 on the (**left**) and 2023 on the (**right**)).

2.3.6. Stable Hydroxide Isotope Sample Collection and Determination

The soil water sampling was conducted using a soil auger to collect soil samples from depths of 0 to 100 cm. These samples were separated into five layers: 0 to 20 cm, 20 to 40 cm, 40 to 60 cm, 60 to 80 cm, and 80 to 100 cm. The samples were then promptly placed in brown glass bottles and stored in a freezer. Water samples were collected from sunflower xylem in chlorophyll-free rhizomes, where there was no transpiration and isotope fractionation. The samples were specifically extracted from the rhizomes of sunflowers located 3~5 cm below the soil surface. During the reproductive phase, samples were taken between 11:00 and 14:00 h on sunny days. These samples were then placed in brown glass bottles and stored in a fridge. Water for irrigation was gathered in glass bottles. Specimens were collected one day before and 4–5 days after each irrigation. The determination was conducted at the Hydrogen and Oxygen Isotope Laboratory of the Institute of Pastoral Water Resources Science, Ministry of Water Resources, located in Hohhot, China. The soil water and wood water were extracted using a plant–water–soil water vacuum extraction system (LI-2000, LICA, Beijing, China) using vacuum low-temperature distillation. The water samples that were obtained were analyzed to determine the stable hydrogen and oxygen isotope compositions. This analysis was conducted using a liquid isotope analyzer (LGR-DRT-100, Los Gatos Research Co., Ltd, USA) according to the following formula:

$$\delta^{18}O(\delta D) = \left(\frac{R_{sample}}{R_{standard}} - 1\right) \times 1000‰ \quad (6)$$

where R_{sample} is the isotope ratio of the sample and $R_{standard}$ is the isotope ratio of the standard; and the precision of $\delta^{18}O$ is ±0.2‰ and the precision of δD is ±0.6‰.

The depth of water absorption by sunflowers and the quantity of water retrieved from each soil layer were determined using a Bayesian mixture model known as the

MixSIAR model. This model was used to compute the contribution of each soil layer to the total water. The R language was used to develop a Bayesian mixture model that incorporates uncertainty from various moisture sources, isotopic signatures, and isotopic fractionation [35].

Before using the MixSIAR model, it is essential to make modifications to the following files: mix-data.txt (file containing plant xylem water data), and mean-source.txt (file containing isotopic data of possible water sources), SD-source.txt (file containing standard deviation values of prospective water sources), and mean-frac.txt (file containing fractionation coefficients, typically set to 0). To optimize the model's performance, it was executed for 1,000,000 iterations. Subsequently, the density was examined in the diagnostics window to see whether it was below 0.01. If the density exceeded 0.01, the number of iterations was incremented until the density fell below 0.01. The model was executed at this juncture to obtain the optimal outcomes.

2.3.7. Data Analysis

We organized the data using Microsoft Excel 2016 and generated graphs using Origin 2022 Pro. We employed analysis of variance (ANOVA) to assess the impact of different irrigation levels on sunflower physiological indicators and conducted post hoc pairwise comparisons using the LSD method to determine significant differences.

2.4. HYDRUS-2D Model

2.4.1. Model Fundamentals

The HYDRUS-2D model (https://www.pc-progress.com/en/Default.aspx?hydrus-1d, accessed on 13 May 2024) was used to replicate the movement of water and salt in the soil under varying irrigation rates in a sunflower agricultural area. The HYDRUS-2D model employs the modified Richards equation [36] to depict the control equation for two-dimensional unsaturated water flow, referred to as Equation (7):

$$\frac{\partial \theta}{\partial t} = \frac{\partial}{\partial x}\left[K(h)\frac{\partial h}{\partial x}\right] + \frac{\partial}{\partial z}\left[K(h)\left(\frac{\partial h}{\partial z} + 1\right)\right] - S(h) \tag{7}$$

where θ is the volumetric water content, $cm^3 \cdot cm^{-3}$; t is the time, d; $K(h)$ is the unsaturated hydraulic conductivity, $cm \cdot d^{-1}$; h is the soil water potential, cm; x and z are the horizontal and vertical distances, cm; and $S(h)$ is the rate of water uptake by the root system, $cm \cdot d^{-1}$.

Soil moisture infiltration was described by the Van Genuchten model [37], Equation:

$$\theta(h) = \begin{cases} \theta_r + \frac{\theta_s - \theta_r}{\left(1 + |\alpha h|^n\right)^m} & (h < 0) \\ \theta_s & (h \geq 0) \end{cases} \tag{8}$$

$$K(h) = K_S S_e^l \left[1 - \left(1 - S_e^{\frac{1}{m}}\right)^m\right]^2 \tag{9}$$

$$m = 1 - \frac{1}{n} \tag{10}$$

where θ_s is the soil saturated water content, $cm^3 \cdot cm^{-3}$; θ_r is the soil residual water content, $cm^3 \cdot cm^{-3}$; $\theta_{(h)}$ is the soil relative saturation, $cm^3 \cdot cm^{-3}$; K_S is the soil saturated hydraulic conductivity, $cm \cdot h^{-1}$; S_e is the soil relative saturation; and α, n, and l are empirical coefficients.

The movement of salt in soil is affected by convection and hydrodynamic dispersion. The model utilizes the convection–dispersion equation to explain salt transport [38], which is represented by the following equation:

$$\frac{\partial(\theta_C)}{\partial_t} = \frac{\partial}{\partial_x}\left(\theta D_T \frac{\partial_C}{\partial_x}\right) + \frac{\partial}{\partial_z}\left(\theta D_L \frac{\partial_C}{\partial_Z}\right) - \frac{\partial(q_i c)}{\partial_Z} - S(h) \tag{11}$$

where c is the soil salt concentration, g·cm^{-3}; q_i is the water flux, cm·d^{-1}; D_T is the transverse diffusion coefficient, cm^2·d^{-1}; and D_L is the longitudinal diffusion coefficient, cm^2·d^{-1}.

2.4.2. Water Absorption by Roots

Root water uptake was modeled using the Feddes model [39] with Equation (12):

$$S(h) = \alpha(h) b(x,z) T_p L \tag{12}$$

where $\alpha(h)$ is the water stress coefficient; $b(x, z)$ is the root water uptake distribution density function, determined according to the actual root distribution; T_p is the potential transpiration rate, cm·d^{-1}; and L is the maximum soil surface width of the root zone distribution, cm.

The water stress function was taken as follows:

$$\alpha(h) = \begin{cases} \frac{h_1 - h}{h_1 - h_2} & h_2 < h \le h_1 \\ 1 & h_2 \le h \le h_1 \\ \frac{h - h_4}{h_3 - h_4} & h_4 \le h \le h_3 \end{cases} \tag{13}$$

where h_1 (cm) is the pressure head at which roots begin to extract water from the soil, set at -15 cm; h_2 is the pressure head below which roots extract water at the maximum rate, set at -350 cm; h_3 is the limiting pressure head at which roots are unable to extract water at the maximum rate, set at -700 cm; and h_4, also known as the wilting pressure head, is the pressure head at which roots are unable to absorb water, set at -8000 cm. It was set to -8000 cm. Sunflower-specific values were obtained from the HYDRUS database.

2.4.3. Model Initial Boundary Conditions

The simulation area has a rectangular shape with a width of 60 cm and a depth of 150 cm. The upper boundary is partially covered with a semi-film, while the saturated head boundary is located at the drip head during drip irrigation. The region covered with film represents a zero-flux boundary, while the piece not covered with film represents an atmospheric boundary. In the simulation region, the subterranean water reaches a maximum depth of 138.4 cm. As a result, the bottom boundary is defined as the saturated head boundary, while the left and right borders are symmetric surfaces on both sides, with zero flux limits. Figure 5 illustrates the simulation area of the model.

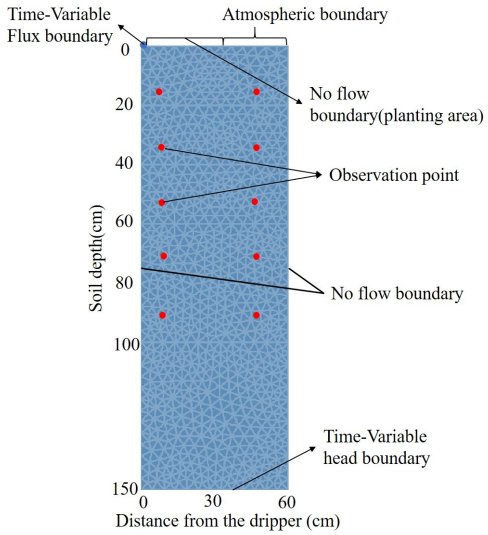

Figure 5. Schematic of modeling area, observation points, and boundary conditions.

2.4.4. Model Parameter

The Rosetta module was used to forecast the soil hydraulic parameters (θs, θr, n, m, and Ks) based on the dry bulk weight, sand content, powder content, and clay content of the soil. These predictions were then calibrated by comparing the simulated values with the observed values of soil moisture and salt content. The soil's longitudinal dispersion was adjusted to a range of 30–60 cm, while the lateral dispersion was set to one-tenth of the longitudinal dispersion. In this investigation, the molecular diffusion coefficient was assumed to be 0 due to its often insignificant nature. Soil hydraulic parameter values are shown in Table 2.

Table 2. Amended soil hydraulic parameter values.

Soil Layer (cm)	θ_r ($cm^3 \cdot cm^{-3}$)	θ_s ($cm^3 \cdot cm^{-3}$)	α (cm^{-1})	n (Dimensionless)	K_S ($cm \cdot d^{-1}$)	l (Dimensionless)
0–20	0.0252	0.381	0.011	1.224	10.84	0.5
20–40	0.0353	0.382	0.015	1.212	15.42	0.5
40–60	0.0485	0.465	0.024	1.351	24.96	0.5
60–100	0.0494	0.484	0.019	1.423	24.97	0.5
100–150	0.0658	0.492	0.016	1.451	41.24	0.5

2.4.5. Model Performance Evaluation

The model parameters were initially calibrated using soil water salinity content measurements in 2022. Subsequently, the model was validated using data from 2023. The accuracy of the model was assessed using the coefficient of determination (R^2), root mean square error (RMSE), and mean absolute error (MAE). These metrics were calculated using the respective formulae.

$$R^2 = 1 - \frac{\sum_{i=1}^{N}|S_i - M_i|}{\sum_{i=1}^{N}|S_i - M_{avg}|} \quad (14)$$

$$RMSE = \left|\frac{\sum_{i=1}^{N}(S_i - M_i)^2}{N}\right|^{\frac{1}{2}} \quad (15)$$

$$MAE = \frac{1}{N}\sum_{i=1}^{N}|M_i - S_i| \quad (16)$$

where S_i and M_i represent the measured and model-simulated values in the field, respectively; N denotes the number of measured values; and M_{avg} is the average of the actual values.

3. Results

3.1. Model Evaluation

To verify the accuracy of the HYDRUS-2D model, we inputted the soil water content and salinity data acquired in 2022 into the model. This allowed us to determine the factors related to the soil moisture characteristics. In 2023, we verified the model using the measured soil water content data. We calculated the coefficient of determination (R^2), root mean square error (RMSE), and mean absolute error (MAE) to compare the simulated and measured values of soil water and salinity. These comparisons were made for different drip irrigation water treatments in both 2022 and 2023. The results can be found in Table 3. In Table 3, the coefficient of determination (R^2) for the measured and simulated values varied from 0.85 to 0.99. The root mean square error (RMSE) ranged from 0.014 to 0.112 $cm^3 \cdot cm^{-3}$, and the mean absolute error (MAE) ranged from 0.011 to 0.152 $cm^3 \cdot cm^{-3}$. The overall fit was satisfactory. The inaccuracies in soil water content and salinity were greater in the 0 to 40 cm depth range compared to the 40 to 100 cm depth range, based on the measured and simulated data of the rate and validation years. This was mostly due to the greater impact of irrigation and rainfall on the uppermost layer of the soil. Nevertheless, the discrepancies between the measured and simulated values fall within the acceptable range, suggesting that the HYDRUS-2D model is capable of accurately simulating soil water and salt content

under various drip irrigation volumes. Therefore, it can be utilized to conduct simulations and analyze experiments related to this paper.

Table 3. Measurement of soil water content and soil salinity statistics for the years 2022 (calibration) and 2023 (validation).

Treatment	Parameter	Error	2022 (Calibration)				2023 (Validation)			
			0~20 cm	20~40 cm	40~60 cm	60~100 cm	0~20 cm	20~40 cm	40~60 cm	60~100 cm
HW	SWC	R^2	0.85	0.88	0.89	0.89	0.90	0.98	0.98	0.88
		RMSE ($cm^3 \cdot cm^{-3}$)	0.051	0.042	0.041	0.078	0.094	0.108	0.071	0.043
		MAE ($cm^3 \cdot cm^{-3}$)	0.012	0.022	0.034	0.041	0.081	0.118	0.152	0.102
	SSC	R^2	0.85	0.92	0.89	0.88	0.96	0.97	0.95	0.98
		RMSE ($g \cdot kg^{-1}$)	0.041	0.075	0.076	0.052	0.063	0.071	0.021	0.014
		MAE ($g \cdot kg^{-1}$)	0.071	0.084	0.071	0.065	0.082	0.071	0.091	0.072
MW	SWC	R^2	0.87	0.85	0.88	0.87	0.89	0.88	0.88	0.89
		RMSE ($cm^3 \cdot cm^{-3}$)	0.042	0.061	0.042	0.025	0.037	0.055	0.075	0.024
		MAE ($cm^3 \cdot cm^{-3}$)	0.026	0.046	0.072	0.61	0.02	0.04	0.05	0.02
	SSC	R^2	0.89	0.89	0.96	0.99	0.88	0.87	0.89	0.97
		RMSE ($g \cdot kg^{-1}$)	0.054	0.035	0.042	0.055	0.024	0.056	0.048	0.064
		MAE ($g \cdot kg^{-1}$)	0.088	0.087	0.084	0.075	0.081	0.071	0.075	0.080
LW	SWC	R^2	0.88	0.87	0.91	0.89	0.89	0.90	0.89	0.91
		RMSE ($cm^3 \cdot cm^{-3}$)	0.016	0.015	0.015	0.021	0.024	0.022	0.015	0.017
		MAE ($cm^3 \cdot cm^{-3}$)	0.021	0.024	0.031	0.027	0.051	0.041	0.042	0.052
	SSC	R^2	0.87	0.89	0.89	0.87	0.87	0.96	0.99	0.89
		RMSE ($g \cdot kg^{-1}$)	0.093	0.103	0.089	0.096	0.112	0.099	0.089	0.095
		MAE ($g \cdot kg^{-1}$)	0.091	0.089	0.084	0.075	0.084	0.091	0.088	0.071

3.2. Effect of Different Drip Irrigation Water Rates on Soil Water Content

Figure 6 displays a comparative examination of soil water content across three treatments, namely, in the range of 0 to 100 cm. During the reproductive period of sunflowers, the soil water content from 0 to 40 cm exhibited a pattern of "high–low–medium". The soil water content from 40 to 100 cm was less influenced by the crop's root system and the depth of the underground water was relatively shallow. As a result, the fluctuation in soil water content was minimal. The soil water content in the 40–100 cm depth range was hardly influenced by the crop root system. Additionally, the groundwater level was close to the surface, resulting in a modest variation in soil water content, which stayed within the range of 0.3 $cm^3 \cdot cm^{-3}$ to 0.4 $cm^3 \cdot cm^{-3}$.

Figure 6 demonstrates that the soil water content of the HW treatment was greater than that of the MW and LW treatments. During the reproductive period in 2022, the HW treatment exhibited a 3.6% and 4.4% increase in water content at a depth of 0–20 cm compared to the MW and LW treatments, respectively. Similarly, at a depth of 20–40 cm, the HW treatment had a 1.9% and 3.0% higher water content than the MW and LW treatments. By mid-2023, the HW treatment exhibited a 6.0% and 4.68% increase in soil water content at a depth of 0–20 cm compared to the MW and LW treatments. Similarly, at a depth of 20–40 cm, the HW treatment showed a 1.9% and 3.0% increase in soil water content compared to the MW and LW treatments, respectively, with a difference of 3.2% and 3.0%. During the years 2022 and 2023, the soil water content in the top 20 cm of soil increased by 11.7% to 17.9% after a single irrigation for 3 days in the HW treatment compared to the MW treatment, and by 19.3% to 26.9% compared to the LW treatment. Similarly, in the 20–40 cm

soil layer, the HW treatment had a 12.2% to 25.1% higher soil water content compared to MW and LW treatments, and an 11.3% to 15.4% higher soil water content compared to the 40–100 cm soil layer. However, the differences in soil water content between the HW, MW, and LW treatments in the 40–100 cm soil layer were small and almost indistinguishable ($p > 0.1$).

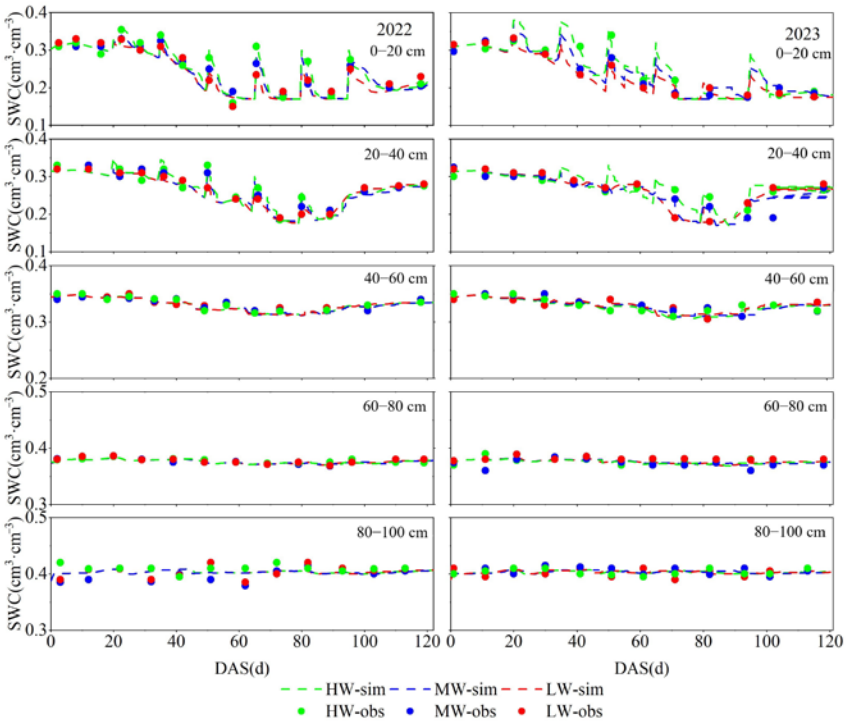

Figure 6. Changes in soil water content from 0–20 cm, 20–40 cm, 40–60 cm, 60–80 cm, and 80–100 cm in the years 2022 (**left**) and 2023 (**right**).

3.3. Effect of Different Drip Irrigation Water Rates on Water Uptake and Yield of Sunflower

The study utilized a MixSIAR Bayesian isotope mixing model to measure the proportion of soil water that contributed to crop water under different treatments and at various depths during the fertility periods of sunflowers in 2022 and 2023. Additionally, the model was used to identify the primary depth at which sunflower roots absorbed water during each fertility stage, as depicted in Figure 7. The water absorption by sunflower roots varied between 2022 and 2023, influenced by temperature and rainfall. This difference was observed in the range of 0–40 cm of soil ($p < 0.05$). However, there was no significant difference in the contribution of deep soil water ($p > 0.05$). The main source of water in the 60–100 cm soil depth was underground water, accounting for 60.5–82.7%. In both years, the general patterns of root water uptake were comparable. Therefore, this article employed the average data from the two years for descriptive analysis. The findings indicated that the mean proportions of soil water input for the whole fertility period at depths of 0–20 cm, 20–40 cm, 40–60 cm, 60–80 cm, and 80–100 cm were 0.273, 0.225, 0.197, 0.171, and 0.134, respectively. As the soil layer's depth climbed, the amount of soil water reduced proportionally. Sunflowers mostly require soil water at the 0–40 cm depth during the seedling and elongation stages, and within the 20–80 cm depth during the grouting and maturity stages.

Varying drip irrigation rates demonstrated distinct impacts on water absorption throughout different growth stages of sunflowers. During the seedling period, all treatments primarily absorbed water from the 0~40 cm soil layer, with contribution values ranging from 0.541 to 0.625. There was no significant difference in water uptake between the HW and MW treatments ($p > 0.05$), but the LW treatment differed significantly from both ($p < 0.05$). Similarly, during the grouting period, the HW treatment mainly sourced water from the 20~40 cm soil layer with a contribution value of 0.341, while the MW and LW

treatments sourced water from the 0~20 cm and 60~80 cm soil layers with a contribution value greater than 0.240. Finally, during the ripening stage, the HW treatments absorbed water from the 0~20 cm and 60~80 cm soil layers, while the MW and LW treatments primarily absorbed water from the 0~80 cm soil layer, with a relatively even distribution among the soil layers.

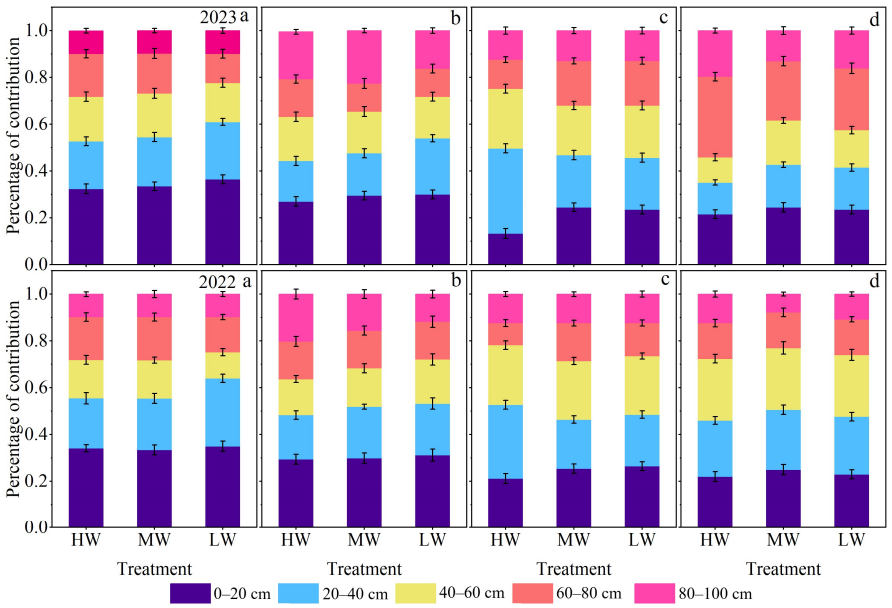

Figure 7. Proportion of water contribution from different soil depths in 2022 (**bottom**) and 2023 (**top**) (a, b, c, and d denote seedling, nodulation, irrigation, and maturity stages of sunflower, respectively).

The impact of various amounts of drip irrigation on the production and water usage efficiency of sunflowers was observed and documented in Figure 8. Both years showed a significant difference ($p < 0.05$) between HW and both MW and LW treatments. However, there was no difference between MW and LW treatments. The average yield values for HW, MW, and LW treatments were 5069 kg·ha^{-1}, 4396 kg·ha^{-1}, and 4370 kg·ha^{-1}, respectively. The HW treatment had a yield that was 15.3% and 16.0% higher than the MW and LW treatments, respectively. In terms of water use efficiency, there was a significant difference ($p < 0.05$) among the three treatments. The two-year mean values for water use efficiency were 1.108, 0.991, and 1.028 for the HW, MW, and LW treatments, respectively.

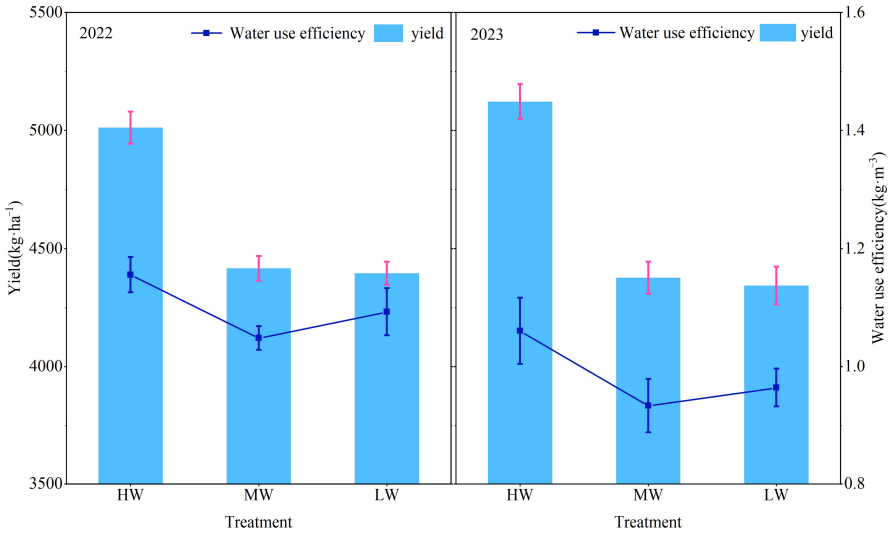

Figure 8. Yield and water use efficiency of sunflower across treatments in 2022 (**left**) and 2023 (**right**).

3.4. Effect of Different Drip Irrigation Water Rates on Soil Salinity Content

The soil salinity measurements for the HW, MW, and LW treatments at depths of 0 to 100 cm in 2022 and 2023 are shown in Figure 9. The soil salinity of sunflower plants fluctuated within the 0 to 100 cm depth range throughout the reproductive phase. These fluctuations varied at various periods of the reproductive cycle. The mean soil salinity from the 0 to 20 cm depth in the HW, MW, and LW treatments throughout the reproductive phase of sunflowers in 2022 and 2023 was 5.89 and 5.59, respectively. Following a single irrigation, the leaching impact of the irrigation water caused the movement of soil salt to deeper layers. As a result, the average salinity of the 0–20 cm soil in each treatment reduced by 8.1% to 22.0% three days after irrigation in both 2022 and 2023. Upon reaching maturity, as the crop's physiological activity decreased, the soil water content became more consistent. An analysis of two years' worth of data revealed that the salt levels at the soil surface varied from 6.5 $g \cdot kg^{-1}$ to 9.3 $g \cdot kg^{-1}$.

There were no significant differences ($p > 0.05$) in the salinity content of the top layer of soil (0–20 cm) during the entire growth period of the sunflower when different amounts of drip irrigation water were used under the membrane. However, there were significant differences ($p < 0.05$) in the salinity content of the top layer of soil after a single irrigation in the high-water (HW), medium-water (MW), and low-water (LW) treatments. An analysis of data from 2022 and 2023 showed that irrigation resulted in a reduction in the average salinity of the 0–20 cm soil layer. Specifically, the salinity dropped by 7.0% and 10.8% for the high-water (HW) treatment compared to the medium-water (MW) and low-water (LW) treatments, and by 4.05% for the MW treatment compared to the LW treatment. During the initial and final stages of the reproductive period, the average salinity of the 0–20 cm soil rose by 109.2%, 111.7%, and 111.6% in both years under the high-water (HW), medium-water (MW), and low-water (LW) treatments, respectively.

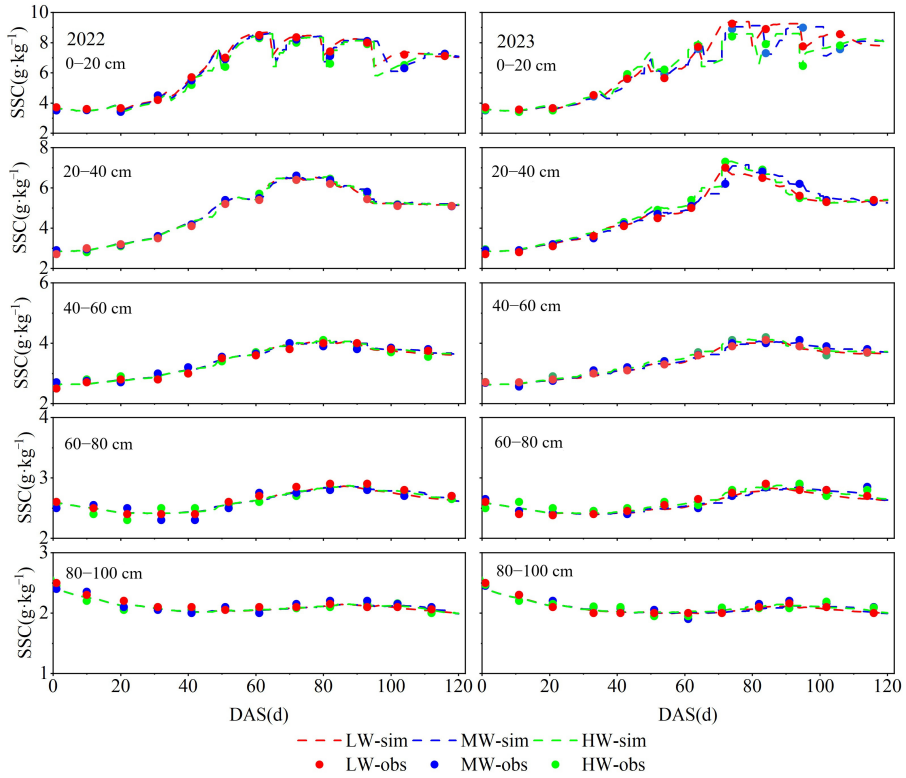

Figure 9. Changes in soil salinity from 0–20 cm, 20–40 cm, 40–60 cm, 60–80 cm, and 80–100 cm in the years 2022 (**left**) and 2023 (**right**).

3.5. Effect of Different Drip Irrigation Water Rates on Soil Salinity Distribution

The dynamics and dispersion of soil salinity in 2022 and 2023 exhibit similarities, with 2022 serving as the benchmark year and 2023 as the validation year. Therefore, the data from 2023 have more representativeness. Hence, this article primarily examines the dispersion of soil salinity in 2023 in the absence of drip irrigation. Figure 10 illustrates the spatial arrangement of soil salt in the year 2023. The fluctuations in soil salinity mostly occurred at the 0~30 cm depth below the drip line and the root zone of sunflowers. This was primarily due to the influence of irrigation and the absorption of water by the roots.

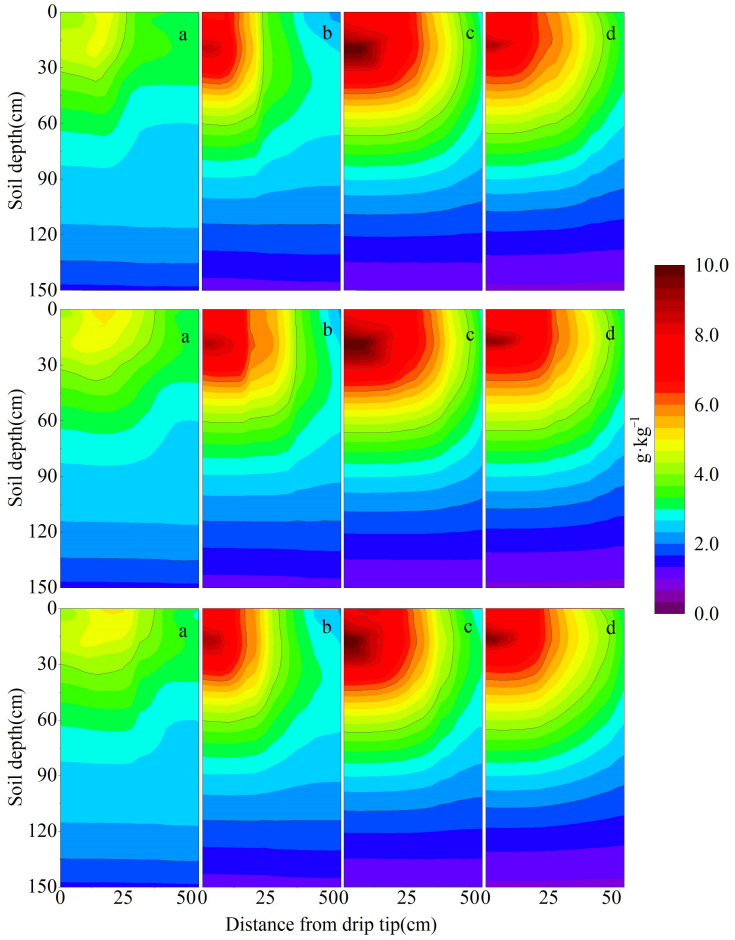

Figure 10. Effect of three different amounts of drip irrigation water under membrane (HW, MW, and LW) on soil salinity distribution in 2023 (a, b, c, and d denote the salinity distribution of sunflower at seedling, nodulation, irrigating, and maturity 3 days after irrigation, respectively).

The soil salt content in the 0~20 cm, 20~40 cm, 40~60 cm, and 60~100 cm depths after irrigation ranged between 3.1~10.8 g·kg^{-1}, 2.9~6.9 g·kg^{-1}, 2.6~4.1 g·kg^{-1}, and 1.0~2.8 g·kg^{-1}, respectively. The irrigation and root water absorption had little impact on the soil salinity in the extracellular area, whereas rainfall and evaporation were the primary factors influencing it. The extracellular area of the soil had salt values ranging from 2.7 to 4.8 g·kg^{-1}, 2.8 to 4.0 g·kg^{-1}, 2.7 to 3.4 g·kg^{-1}, and 1.7 to 2.6 g·kg^{-1} at depths of 0 to 20 cm, 20 to 40 cm, 40 to 60 cm, and 60 to 100 cm, respectively. The intramembrane area fell by 13.1~55.5%, 0.7~42.8%, −0.4~16.2%, and −72.7~7.5% in units of g·kg^{-1}. The significance analysis reveals a substantial difference in the salt concentration of soil within and outside the barrier. The soil outside the membrane, within a depth of 0~60 cm, has a lower salt concentration compared to the soil within the membrane. However, the soil inside the membrane, within a depth of 60~100 cm, has a lower salt content compared to the soil outside the membrane. The primary factor is the accumulation of soil salt in the

intermediate layer of the soil surface (0–60 cm) due to water, which is not washed away to the deeper layer of the soil (60–100 cm) by drip irrigation water. Throughout the whole development period of the sunflower, there was no notable disparity in soil salinity across the three different volumes of drip irrigation ($p > 0.05$).

3.6. Effect of Different Drip Irrigation Water Volumes on Water–Salt Balance

The water–salt balance for each irrigation treatment in the experimental years is shown in Table 4. Varying levels of drip irrigation applied underneath the membrane had a more pronounced impact on the soil's water–salt equilibrium. The cost of the HW treatment increased by an average of 3.0% and 7.6% in the two years compared to the MW and LW treatments, respectively. In 2022, the ET_C was 11.4% higher compared to 2023. Additionally, under the HW treatment, the amount of underground water recharge was 18.4% lower than in 2023. The ETC of the HW treatment was also 11.4% higher than in 2023, while the amount of groundwater recharge was 18.4% lower. In comparison to the year 2023, the evapotranspiration coefficient (ET_C) was 11.3% and 12.0% greater in the medium-water (MW) and low-water (LW) treatments, respectively. Additionally, the groundwater recharge was 17.4% and 14.9% lower in the MW and LW treatments, respectively. The primary factor for this was the significant impact of precipitation, which amounted to 127.2 mm during the reproductive phase of sunflower in the year 2023, representing just 63.0% of the rainfall seen during the reproductive phase of sunflower in the year 2022.

Table 4. Agricultural soil moisture and salt balance of HW, MW, and LW during sunflower fertility in 2022 and 2023. P is rainfall (mm), I is irrigation (mm), ET_C is water consumed by the farmland (mm), G is groundwater recharge (mm), and ΔW is soil water storage (mm); S_i is the initial soil salinity ($t \cdot ha^{-1}$), S_f is soil salinity at the end of the reproductive period ($t \cdot ha^{-1}$), S_d is the salinity recharged to the soil by the groundwater ($t \cdot ha^{-1}$), and S_p is the salinity that enters the farmland with the irrigation water($t \cdot ha^{-1}$).

Year	Treatment	Water Balance (mm)					Salt Balance ($t \cdot ha^{-1}$)			
		P	I	ET_C	G	ΔW	S_i	S_f	S_d	S_p
2022	HW	201.8	162	483.2	115	−4.4	4.056	5.752	0.74	0.956
	MW	201.8	135	468.9	128	−4.1	4.045	5.793	0.951	0.797
	LW	201.8	108	450.5	137	−3.7	3.992	5.767	1.138	0.637
2023	HW	127.2	162	433.8	141	−3.6	4.002	6.111	1.153	0.956
	MW	127.2	135	421.4	155	−4.2	3.998	6.117	1.332	0.797
	LW	127.2	108	402.3	161	−6.1	4.015	6.125	1.473	0.637

The initial soil salinity refers to the soil salinity measured 2 days before planting following the spring irrigation. All experimental plots received a spring irrigation of 180 mm, which was applied 10 days before sowing. The disparity in the initial soil salinity levels between the two years was minimal, fluctuating between 3.992 and 4.056 $t \cdot ha^{-1}$. However, by the conclusion of the sunflower fertility period, the soil salinity escalated to 5.752–6.125 $t \cdot ha^{-1}$, representing a substantial increase of 41.8–52.7%. This surge in salinity can be attributed primarily to the replenishment of underground water and irrigation water. The recharge of salt from underground water contributed to 43.6–69.8% of the overall increase in salt levels. Specifically, the increase in groundwater salinity resulting from the HW treatment in 2022 was less than 50% of the total increase. Consequently, the main goal of addressing the soil salinity issue in the area is to reduce the rise in groundwater salinity.

3.7. HYDRUS-2D Model for Scenario Simulation

The HYDRUS-2D model accurately predicted the experimental treatments, since the prediction results closely matched the observed data. The HYDRUS-2D model was employed to simulate the average soil water content, salt accumulation rate, and salt rebound time for sunflowers during various fertility periods. The simulations were conducted using

five different irrigation quotas of 15 mm, 20 mm, 25 mm, 30 mm, and 35 mm. All other data remained consistent with the 2023 dataset.

Figure 11 displays the outcomes of the simulation. The mean soil water content rises in proportion to the irrigation rate. During the reproductive phase of sunflower growth, the average water content between 0 and 40 cm reaches its minimum value during the irrigation period. This period is critical for sunflower growth and requires a higher water demand. The rate of soil salinity accumulation varied during different fertility periods of sunflowers and with different amounts of irrigation water. Soil salinity increased during the seedling, elongation, and grouting periods, reaching its peak during the grouting period. However, salinity appeared to decline during the maturity period, primarily due to the reduced physiological activity of sunflowers and decreased water uptake by the root system. Additionally, the decrease in temperature during this period led to a decrease in soil moisture evaporation. Earth's uppermost layer of loose material, composed of minerals, organic matter, and air, supports plant growth and is essential for agriculture. The level of surface aggregation of salinity was reduced.

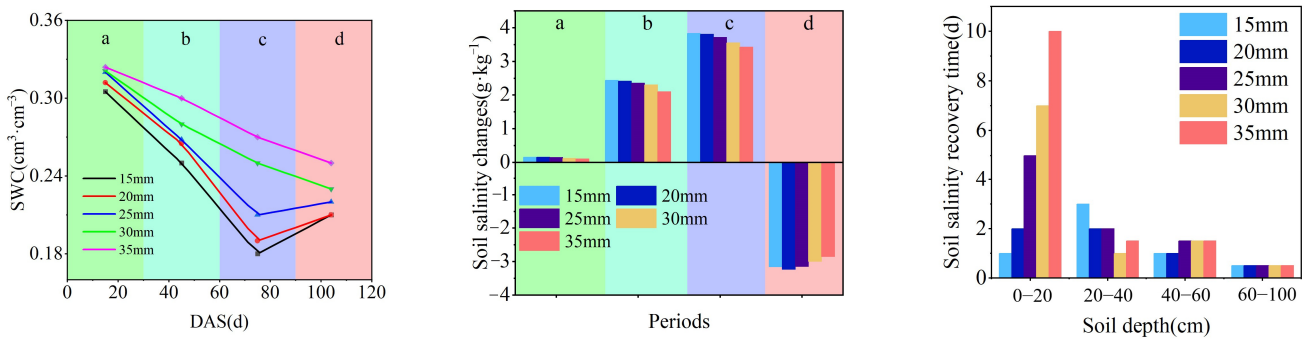

Figure 11. Changes in soil water content and salt accumulation under 15 mm, 20 mm, 25 mm, 30 mm, and 35 mm irrigation at different fertility stages of sunflower (a, b, c, and d in the figure are at seedling, nodulation, irrigating and maturity stages of sunflower, respectively) and the time of salinity rebound.

The storage of soil salt at depths of 0 to 40 cm decreased as the amount of irrigation water increased. The salinity of the soil also increased during the sunflower seedling period, elongation period, and irrigation period. The increase in salinity was measured at 0.1–0.15 g·kg^{-1}, 2.1–2.44 g·kg^{-1}, and 3.42–3.83 g·kg^{-1}, respectively. The treatment with an irrigation quota of 20 mm during the maturity period resulted in the greatest decrease in salinity, measuring 3.24 g·kg^{-1}. The recovery time for soil salinity ranged from 1 to 10 days. The time required for soil salinity to recover from 0 to 20 cm was the longest and had a positive correlation with the amount of irrigation water. The slowest recovery time for soil salinity from 0 to 40 cm was observed with the 15 mm treatment, while the fastest recovery time was observed with the 30 mm treatment. The recovery time for soil salinity from 40 to 60 cm was 1–2 days. The recovery time for soil salinity from 60 to 100 cm was influenced by groundwater, resulting in a reduction in soil salinity from 3.24 to 3.83 g·kg^{-1} and 3.42 to 3.83 g·kg^{-1}, respectively, during the ripening stage. The soil experienced the influence of subterranean water, resulting in a salinity recovery period of around 24 h.

4. Discussion

4.1. Effect of Different Drip Irrigation Water Levels on Soil Moisture

Implementing effective water conservation measures is crucial for safeguarding the soil and water ecosystem and mitigating soil erosion in dry regions [40]. By using a logical approach to the exploitation of water resources, it is possible to maintain soil moisture levels and support crop development, hence enhancing agricultural output [41]. Both measured and simulated data indicated that the water content of the soil in the 0~40 cm depth range of sunflower plants exhibited significant changes ($p < 0.05$) when subjected to

varied volumes of irrigation water under drip irrigation with a membrane. However, there was no significant difference ($p > 0.05$) in the water content of the soil in the 40~100 cm depth range. During different fertility periods, the water content of the soil layer between 0 and 40 cm exhibited varying changes. In the seedling period, evaporation was not intense and the root system had a weak ability to absorb water, resulting in a high soil water content. In the elongation period and irrigation period, the soil water content was low due to the increased air temperature and strong crop physiological activity, which demanded a large amount of soil water. In the maturity period, the crop physiological activity decreased and the air temperature gradually declined, leading to an increase in the soil water holding capacity.

The irrigation region located on the southern bank of the Yellow River employs border irrigation as a year-round method for irrigating crops. This practice helps maintain a shallow depth of subsurface water [42]. Subterranean aquifers play an essential role in the natural cycle of water on agricultural land [43]. Measuring the amount of water that enters subsurface sources is crucial for the establishment of effective irrigation systems. Prior studies have examined the quantity of groundwater recharge using both measured data and modeling studies. These studies have described the interdependent interaction between soil water and groundwater [43,44]. Nevertheless, relying solely on a single method for the computational analysis of underground water utilization is insufficient to precisely assess the role of underground water in agricultural production. Therefore, this study employed the HYDRUS-2D model and stable hydroxide and oxygen isotope methods to analyze crop utilization in underground water. This approach aims to address the limitations of previous studies and provide a more comprehensive understanding of the subject. Significant differences in the recharge of soil water content and underground water were observed based on varying amounts of irrigation water. These differences can be attributed to the decrease in capillary force in the shallow buried groundwater area as the irrigation volume increases. As a result, the soil water potential in deeper soil becomes larger, causing the upward recharge of the deeper soil water when irrigation volume is lower. Additionally, changes in irrigation water volume affect the utilization of soil water by the crop root system, leading to differences in water uptake. These findings were supported by the HYDRUS-2D model and stable hydroxide isotope method. The finding was corroborated by isotope readings. The use of the HW treatment resulted in greater water consumption in the uppermost soil layer (0–40 cm), while the MW and LW treatments were mostly influenced by the quantity of irrigation water. The insufficient topsoil moisture throughout the reproductive stage of the sunflower resulted in the root system descending and absorbing soil moisture from a depth of 60–80 cm. The research conducted by Dou [45] indicated that sunflowers mostly absorb water from a depth of 0–60 cm. The primary factor contributing to the disparity may be attributed to the irrigation method employed in this study, which followed the principle of "frequent, small amounts". In contrast, Dou utilized a single large irrigation event. Additionally, the experimental area experienced relatively low rainfall, resulting in an increased need for sunflowers to access water from deeper soil layers during their main reproductive phase. The simulation of the HYDRUS model revealed that the soil water content at a depth of 60–80 cm remained relatively stable. This can be attributed to the slow absorption of soil water by sunflower plants in this layer, which is likely due to the shallow depth of the underground water. As a result, the limited amount of water absorbed by the plants did not lead to a significant change in the overall water content. These findings align with the results reported by Gao and Zhang et al. [46,47]. The sunflower's groundwater usage ranged from 25.49% to 39.21% throughout its reproductive period. This usage varied significantly ($p < 0.05$) among high-water, medium-water, and low-water conditions. The data from hydrogen and oxygen isotopes also confirmed the effectiveness of the HYDRUS-2D model in simulating groundwater movement in shallow burial areas. The model produced accurate results for underground water flow.

4.2. Effect of Different Drip Irrigation Water Rates on Soil Salinity

Efficient water use and effective salt regulation are crucial for the management of farming in arid and semi-arid regions. An analysis of two years' data revealed that, during the seedling period, soil salinity fluctuations were minimal due to the gradual increase in temperature and the limited ability of crop root systems to extract soil moisture, resulting in low soil moisture reduction. However, during the elongation period and filling period, soil salinity became concentrated near the surface due to the evaporation of soil moisture and root absorption. The irrigation water caused a reduction in soil salinity. Inside the membrane, the soil salinity varied from 3.47 to 8.71 $g \cdot kg^{-1}$ from 0 to 40 cm, whereas, outside the membrane, it ranged from 2.75 to 4.52 $g \cdot kg^{-1}$. The salinity inside the membrane was more significantly influenced by irrigation and the absorption of water by the roots, resulting in higher fluctuations compared to the salinity outside the membrane [48]. The volatility of soil salinity reduced as the soil depth increased throughout the reproductive stage of the sunflower. The soil salinity stabilized within the range of 1.99 to 2.99 $g \cdot kg^{-1}$ between the depths of 60 to 100 cm.

Salinity variations were found to be significant only in the uppermost soil layer (0–20 cm) after irrigation with varying volumes of irrigation water, whereas no significant changes in soil salinity were seen in the 20 to 100 cm depth range. This is because drip irrigation enhances the crop root system's response to water, resulting in stronger water infiltration. However, due to the small volume of water used in drip irrigation, it is unable to effectively leach the soil salts below 20 cm. This finding aligns with previous research [49,50]. The assessment of irrigation volume in the shallow buried groundwater region is crucial as it significantly impacts the depth of buried water and the accumulation of soil salts [51]. This paper demonstrates a negative correlation between the quantity of irrigation water and the recharge of salt in groundwater. The recharge of salt in groundwater was significantly different between the LW treatment and the MW and HW treatments ($p < 0.05$). However, increasing the amount of irrigation water led to an increase in the groundwater level, resulting in more recharge of salt from groundwater into the soil. Precipitation has a substantial impact on the development of crops and alterations in the salt levels of soil. During times of heavy precipitation, the replenishment of subterranean water diminishes as the rainfall intensifies, and the accumulation of salts in the groundwater also reduces.

This study utilized the HYDRUS-2D model to simulate a scenario based on previous research [52]. We examined the impact of different irrigation amounts on salt accumulation and the rebound time of soil salts within the soil membrane. Our analysis revealed that these factors had varying effects at different irrigation quotas and fertility periods of sunflowers. The rebound of intramembrane soil salts at a certain time interval indicates the impact of irrigation on enhancing the salinity of the soil between the roots. As the irrigation volume increases, the distance and length of the horizontal soil moisture circulation also increase, leading to a higher concentration of salt. The salinity peak's location progressively migrated downwards as the irrigation water volume increased, aligning with the conclusions reported by Zhang and Ding et al. [53,54]. Reducing the irrigation volume during the pre-fertility stage would result in less leaching of surface soil salts. Increasing the irrigation volume would enhance the time it takes for surface soil salinity to return to normal levels. The increased irrigation volume during the late reproductive stage caused the surface soil salts to be washed down to the 20–60 cm soil layer. This resulted in a lower concentration of salts in the surface soil. However, compared to the treatment with a smaller irrigation volume, the overall time for salt levels to rebound in the 0–60 cm soil layer was reduced. As a result, there were higher salt levels in the rhizosphere. This finding is consistent with a previous study [55] and has practical implications for scenario simulation.

We measured the changes in soil water–salt content in the region where sunflowers are grown, at various rates of irrigation. This was carried out in an area where the subterranean water is located close to the surface. We used the HYDRUS-2D model and hydroxide–oxygen isotope techniques to carry out this analysis. We conducted a study on the dynamics

of water and salt to determine the extent to which various sources of soil water contribute to the development of crops. Unfortunately, our limited monitoring time prevented us from establishing the correlation between the percentage contribution of rainfall and the various hydrological years. Hence, it is essential that we extend the monitoring period to investigate the ratio of rainfall and subsurface water input during water-abundant, flat, and drought years, to establish a logical irrigation system.

5. Conclusions

This research investigates the changes in soil water and salt content in the root zone and the layer where water is absorbed by the roots throughout the reproductive phase of the sunflower. The investigation is conducted using a mix of field tests and numerical simulation. Based on the findings, the following conclusions are drawn:

(1) The coefficient of determination (R^2) between the simulated and measured values of the HYDRUS-2D model, following rate calibration, exceeded 0.85. The root mean square error (RMSE) was less than 0.112 $cm^3 \cdot cm^{-3}$, and the average absolute error (MAE) was less than 0.152 $cm^3 \cdot cm^{-3}$. The model accurately replicates the process of water infiltration in drip irrigation under a shallow groundwater level. The integration of the HYDRUS-2D model with hydrogen and oxygen isotope techniques enables a more comprehensive analysis of water and salt dynamics in crop root zones, as well as root water uptake patterns.

(2) Experimental and simulation results revealed that varying irrigation rates in the shallow underground water burial area led to variations in the water and salt content of the soil layer between 0 and 40 cm. The differences in water and salt content were less pronounced in the soil layer between 40 and 100 cm. When the irrigation rate is low, the root system of sunflowers tends to focus more on the soil layer that is replenished by subterranean water.

(3) The analysis of water–salt balance and scenario simulation revealed a negative correlation between the amount of irrigation water and the amount of underground water recharging soil water and salt. Specifically, under irrigation quotas of 27, 22.5, and 18 mm, the amount of underground water recharging accounted for 28.2%, 32.0%, and 35.2% of the water consumed by the farmland, respectively. Additionally, the amount of underground water recharging salt accounted for 49.2%, 58.5%, and 67.0% of the total increase in the value of salt. When the irrigation quota ranged from 25 to 30 mm, it resulted in a higher crop output and improved efficiency, while also reducing the recharge of salt into the groundwater.

Author Contributions: Conceptualization, C.T. and R.H.; methodology, C.T.; software, J.W.; resources, H.Z.; data curation, R.H. and C.T.; writing—original draft preparation, C.T.; writing—review and editing, C.T. and H.Z. All authors have read and agreed to the published version of the manuscript.

Funding: This research was funded by the [Research on key technologies of drip irrigation for water conservation and efficiency and surface irrigation for salt suppression in Yellow River water] grant number [2021EEDSCXSFQZD011] awarded to Jun Wang.

Data Availability Statement: The data for this study are temporarily unavailable.

Acknowledgments: All the authors thanked the farmers and herders who maintained the experimental fields.

Conflicts of Interest: The authors declare that they have no known competing financial interests or personal relationships that could have appeared to influence the work reported in this paper.

References

1. Wedaa, Z.W.; Abed, S.A.; Ewaid, S.H. The Agricultural Water Footprint of Al-Qadisiyah Governorate, Southern Iraq. *IOP Conf. Ser. Earth Environ. Sci.* **2022**, *1029*, 012025. [CrossRef]
2. Liu, W.; Lei, B.; Liao, J.; Du, L. Spatial and temporal optimal allocation of distributed multiple water sources in irrigation areas. *J. Agric. Eng.* **2022**, *38*, 135–143.

3. Fan, L.; Shi, H.; Li, R. Optimization and sensitivity analysis of border irrigation scheme in Hetao Irrigation District. *J. Agric. Mach.* **2021**, *52*, 280–290.
4. Sun, K.; Zhang, X.W.; Nie, J.; Zou, J.N.; Zhong, X.Y. Evaluation of water resources utilization performance in Chinese provinces and analysis of spatial differentiation and driving factors. *Water Resour. Conserv.* **2023**, *39*, 102–110+186.
5. Jiang, D.; Ao, C.; Bailey, R.T.; Zeng, W.; Huang, J. Simulation of water and salt transport in the Kaidu River Irrigation District using the modified SWAT-Salt. *Agric. Water Manag.* **2022**, *272*, 107845. [CrossRef]
6. Zhu, W.; Yang, J.; Yao, R.; Xie, W.; Wang, X.; Liu, Y. Soil water-salt control and yield improvement under the effect of compound control in saline soil of the Yellow River Delta, China. *Agric. Water Manag.* **2022**, *263*, 107455. [CrossRef]
7. Zhang, W.; Zhou, J.; Feng, G.; Weindorf, D.C.; Hu, G.; Sheng, J. Characteristics of water erosion and conservation practice in arid regions of Central Asia: Xinjiang, China as an example. *Int. Soil Water Conserv. Res.* **2015**, *3*, 97–111. [CrossRef]
8. Boaretto, R.M.; Hippler, F.W.R.; Teixeira, L.A.J.; Fornari, R.C.; Quaggio, J.A.; Mattos, D., Jr. Zinc fertilizers for Citrus production: Assessing nutrient supply via fertigation or foliar application. *Plant Soil* **2023**, *496*, 179–192. [CrossRef]
9. Wang, H.; Wang, N.; Quan, H.; Zhang, F.; Fan, J.; Feng, H.; Cheng, M.; Liao, Z.; Wang, X.; Xiang, Y. Yield and water productivity of crops, vegetables and fruits under subsurface drip irrigation: A global meta-analysis. *Agric. Water Manag.* **2022**, *269*, 107645. [CrossRef]
10. Wang, J.; Du, Y.; Niu, W.; Han, J.; Li, Y.; Yang, P. Drip irrigation mode affects tomato yield by regulating root–soil–microbe interactions. *Agric. Water Manag.* **2022**, *260*, 107188. [CrossRef]
11. Lu, P.; Xing, W.; Yang, Y.; Liu, W.; Luo, W. Simulation of soil water and salt distribution characteristics between strips under drip irrigation with brackish water in shed. *J. Agric. Mach.* **2023**, *54*, 360–371.
12. Bai, S.; Kang, Y.; Wan, S. Winter wheat growth and water use under different drip irrigation regimes in the North China PlainWinter wheat growth and water use under different drip irrigation regimes in the North China Plain. *Irrig. Sci.* **2020**, *38*, 321–335. [CrossRef]
13. Skaggs, T.H.; Trout, T.J.; Šimůnek, J.; Shouse, P.J. Comparison of HYDRUS-2D simulations of drip irrigation with experimental observations. *J. Irrig. Drain. Eng.* **2004**, *130*, 304–310. [CrossRef]
14. Abreu, L.M.M.D.; Quirijn, L.V.J.D. Revisiting the Feddes reduction function for modeling root water uptake and crop transpiration. *J. Hydrol.* **2021**, *603*, 126952.
15. García-Vila, M.; Fereres, E.; Mateos, L.; Orgaz, F.; Steduto, P. Deficit irrigation optimization of cotton with AquaCrop. *Agron. J.* **2009**, *101*, 477–487. [CrossRef]
16. Hassan, J.O.; Shahid, K.; Amer, S.M. Application of the SWAT model to assess climate and land use/cover change impacts on water balance components of the Kabul River Basin, Afghanistan. *J. Water Clim. Change* **2022**, *13*, 3977–3999.
17. Carlos, F.U.; Cristian, K.F.; Marco, G.S.; Mauricio, G.; Humberto, A.; de Miranda Jarbas, H.; Oscar, S.S. Testing the Model Efficiency of HYDRUS 2D/3D Under Desert Conditions for Water Content and Pore Electrical Conductivity: A Case Study in an Olive Orchard. *J. Soil Sci. Plant Nutr.* **2022**, *22*, 1859–1872. [CrossRef]
18. Landry, K.S.O.; Marcel, K.B.; Francois, Z. Water Dynamics under Drip Irrigation to Proper Manage Water Use in Arid Zone. *J. Agric. Chem. Environ.* **2021**, *10*, 57–68.
19. Liu, M.-X.; Yang, J.-S.; Li, X.-M.; Yu, M.; Wang, J. Numerical Simulation of Soil Water Dynamics in a Drip Irrigated Cotton Field Under Plastic Mulch. *Pedosphere* **2013**, *23*, 620–635. [CrossRef]
20. Elnesr, M.; Alazba, A. Computational evaluations of HYDRUS simulations of drip irrigation in 2D and 3D domains (i-Surface drippers). *Comput. Electron. Agric.* **2019**, *162*, 189–205. [CrossRef]
21. Slama, F.; Zemni, N.; Bouksila, F.; De Mascellis, R.; Bouhlila, R. Modeling the impact on root water uptake and solute return flow of different drip irrigation regimes with brackish water. *Water* **2019**, *11*, 425. [CrossRef]
22. Fernández García, I.; Lecina, S.; Ruiz-Sánchez, M.C.; Vera, J.; Conejero, W.; Conesa, M.R.; Domínguez, A.; Pardo, J.J.; Léllis, B.C.; Montesinos, P. Trends and challenges in irrigation scheduling in the semi-arid area of Spain. *Water* **2020**, *12*, 785. [CrossRef]
23. García Morillo, J.; Rodríguez Díaz, J.A.; Camacho, E.; Montesinos, P. Drip irrigation scheduling using HYDRUS 2-D numerical model application for strawberry production in South-West Spain. *Irrig. Drain.* **2017**, *66*, 797–807. [CrossRef]
24. Ruidisch, M.; Kettering, J.; Arnhold, S.; Huwe, B. Modeling water flow in a plastic mulched ridge cultivation system on hillslopes affected by South Korean summer monsoon. *Agric. Water Manag.* **2013**, *116*, 204–217. [CrossRef]
25. Silva, J.A.K.; Šimůnek, J.; McCray, J.E. A modified HYDRUS model for simulating PFAS transport in the vadose zone. *Water* **2020**, *12*, 2758. [CrossRef]
26. Kandelous, M.M.; Šimůnek, J. Numerical simulations of water movement in a subsurface drip irrigation system under field and laboratory conditions using HYDRUS-2D. *Agric. Water Manag.* **2010**, *97*, 1070–1076. [CrossRef]
27. Zhou, J.; Cheng, G.; Li, X.; Hu, B.X.; Wang, G. Numerical modeling of wheat irrigation using coupled HYDRUS and WOFOST models. *Soil Sci. Soc. Am. J.* **2012**, *76*, 648–662. [CrossRef]
28. Bufon, V.B.; Lascano, R.J.; Bednarz, C.; Booker, J.D.; Gitz, D.C. Soil water content on drip irrigated cotton: Comparison of measured and simulated values obtained with the Hydrus 2-D model. *Irrig. Sci.* **2012**, *30*, 259–273. [CrossRef]
29. Li, H.; Zhou, H. Characterization and mechanism of stable isotopes in ecohydrological processes in arid zones. *Arid Zone Geogr.* **2006**, 810–816. [CrossRef]
30. Xing, X.I.; Chen, H.; Zhu, J.J.; Chen, T.T. Water sources of five dominant desert plants in the Nomohon area of the Qaidam Basin. *J. Ecol.* **2014**, *34*, 6277–6286.

31. Pei, Y.; Huang, L.; Shao, M.; Li, R.L.; Zhang, Y.L. Characteristics and influencing factors of soil water recharge at different water table depths in the Maowusu Sandland. *J. Agric. Eng.* **2021**, *37*, 108–116.
32. Allen, R.G.; Pruitt, W.O.; Wright, J.L.; Howell, T.A.; Ventura, F.; Snyder, R.; Itenfisu, D.; Steduto, P.; Berengena, J.; Yrisarry, J.B.; et al. A recommendation on standardized surface resistance for hourly calculation of reference ETo by the FAO56 Penman-Monteith method. *Agric. Water Manag.* **2006**, *81*, 1–22. [CrossRef]
33. Campbell, G.S.; Norman, J.M. The description and measurement of plant canopy structure. *Plant Canopies Growth Form Funct.* **1989**, *1*, 19.
34. Fernández, J.E.; Alcon, F.; Diaz-Espejo, A.; Hernandez-Santana, V.; Cuevas, M.V. Water use indicators and economic analysis for on-farm irrigation decision: A case study of a super high-density olive tree orchard. *Agric. Water Manag.* **2020**, *237*, 106074. [CrossRef]
35. Wu, H.; Zhao, G.; Li, X.Y.; Wang, Y.; He, B.; Jiang, Z.; Zhang, S.; Sun, W. Identifying water sources used by alpine riparian plants in a restoration zone on the Qinghai-Tibet Plateau: Evidence from stable isotopes. *Sci. Total Environ.* **2019**, *697*, 134092. [CrossRef]
36. Richards, L.A. Capillary conduction of liquids through porous mediums. *Physics* **1931**, *1*, 318–333. [CrossRef]
37. Van Genuchten, M.T. A closed-form equation for predicting the hydraulic conductivity of unsaturated soils. *Soil Sci. Soc. Am. J.* **1980**, *44*, 892–898. [CrossRef]
38. Xu, X.; Huang, G.; Sun, C.; Pereira, L.S.; Ramos, T.B.; Huang, Q.; Hao, Y. Assessing the effects of water table depth on water use, soil salinity, and wheat yield: Searching for a target depth for irrigated areas in the upper Yellow River basin. *Agric. Water Manag.* **2013**, *125*, 46–60. [CrossRef]
39. Feddes, R.A. Simulation of field water use and crop yield. In *Simulation of Plant Growth and Crop Production*; Pudoc: Ilocos Sur, Philippines, 1982; pp. 194–209.
40. Wang, G.; Cheng, G.; Xu, Z. Utilization of water resources and its ecological and environmental problems in the arid zone of Northwest China. *J. Nat. Resour.* **1999**, *14*, 109–116.
41. Zhang, X.-Y. Research on water consumption and water-saving irrigation of farmland in typical regions of North China. *Chin. J. Ecol. Agric.* **2018**, *26*, 1454–1464.
42. Ma, J. Prediction of Groundwater Environment Changes by Different Diversion Levels in Hetao Irrigation District, Inner Mongolia. Master's Thesis, Inner Mongolia Agricultural University, Hohhot, China, 2010.
43. Wang, X.; Huo, Z.; Feng, S.; Guo, P.; Guan, H. Estimating groundwater evapotranspiration from irrigated cropland incorporating root zone soil texture and moisture dynamics. *J. Hydrol.* **2016**, *543*, 501–509. [CrossRef]
44. Zhong, Y.; Fei, L.; Fu, Y.; Chen, L.; Liu, L. HYDRUS simulation and validation of soil rising capillary water movement characteristics under the influence of multiple factors. *J. Agric. Eng.* **2018**, *34*, 83–89.
45. Dou, X.; Shi, H.; Li, R.; Miao, Q.; Yan, J.; Tian, F.; Wang, B. Simulation and evaluation of soil water and salt transport under controlled subsurface drainage using HYDRUS-2D model. *Agric. Water Manag.* **2022**, *273*, 107899. [CrossRef]
46. Gao, X.; Bai, Y.; Huo, Z.; Xu, X.; Huang, G.; Xia, Y.; Steenhuis, T.S. Deficit irrigation enhances the contribution of shallow groundwater to crop water consumption in arid areas. *Agric. Water Manag.* **2017**, *185*, 116–125. [CrossRef]
47. Zhang, Y.; Li, X.; Šimůnek, J.; Shi, H.; Chen, N.; Hu, Q. Quantifying water and salt movement in a soil-plant system of a corn field using HYDRUS (2D/3D) and the stable isotope method. *Agric. Water Manag.* **2023**, *288*, 108492. [CrossRef]
48. Zemni, N.; Slama, F.; Bouksila, F.; Bouhlila, R. Simulating and monitoring water flow, salinity distribution, and yield production under buried diffuser irrigation for date palm tree in Saharan Jemna oasis (North Africa). *Agric. Ecosyst. Environ.* **2022**, *325*, 107772. [CrossRef]
49. Guo, Y.; Wang, Q.; Zhao, X.; Li, Z.; Li, M.; Zhang, J.; Wei, K. Field irrigation using magnetized brackish water affects the growth and water consumption of *Haloxylon ammodendron* seedlings in an arid area. *Front. Plant Sci.* **2022**, *13*, 929021. [CrossRef] [PubMed]
50. Wichelns, D.; Qadir, M. Achieving sustainable irrigation requires effective management of salts, soil salinity, and shallow groundwater. *Agric Water Manag.* **2015**, *157*, 31–38. [CrossRef]
51. Aboelsoud, H.M.; Habib, A.; Engel, B.; Hashem, A.A.; Abou El-Hassan, W.; Govind, A.; Elnashar, A.; Eid, M.; Kheir, A.M. The combined impact of shallow groundwater and soil salinity on evapotranspiration using remote sensing in an agricultural alluvial setting. *J. Hydrol. Reg. Stud.* **2023**, *47*, 101372. [CrossRef]
52. Shi, H.B.; Guo, J.W.; Zhou, H.; Wang, G.; Fu, X.; Li, Z. Effects of irrigation volume and groundwater regulation on soil water-salt distribution in arid areas. *J. Agric. Mach.* **2020**, *51*, 268–278.
53. Ding, C.M.; Wu, P.N.; Yue, L.; Li, Y.H.; Guan, X.K.; Wang, T.C. Effects of Hydrus-1D-based simulated tillage on moisture in summer maize fields. *J. Irrig. Drain.* **2020**, *39*, 24–31.
54. Zhang, M.; Yang, P.; Ren, S.; Xu, Z.; Wei, C.; He, X. Effects of irrigation water salinity and irrigation volume on soil water-salt distribution and spring corn growth. *J. Soil Water Conserv.* **2022**, *36*, 290–298.
55. Wang, H.; Zhou, Q.; Zhang, B. Effects of different drip irrigation water volumes on soil salinity in mulched corn fields in Hetao Irrigation District. *J. Irrig. Drain.* **2022**, *41*, 72–83.